Paper 119

©Civil-Comp Press, 2012
Proceedings of the Eighth International Conference
on Engineering Computational Technology,
B.H.V. Topping, (Editor),
Civil-Comp Press, Stirlingshire, Scotland

A Dynamic Wall-Model for Large-Eddy Simulation of High Reynolds Number Shock-Induced Separated Flows

S. Kawai[1] and J. Larsson[2]
[1] Institute of Space and Astronautical Science
Japan Aerospace Exploration Agency, Japan
[2] Center for Turbulence Research
Stanford University, United States of America

Abstract

We propose a simple yet efficient dynamic wall-model for large-eddy simulation (LES) that accurately predicts the turbulent statistics (most importantly, the predicted skin friction) and makes the LES applicable at realistic high Reynolds numbers. The proposed wall model stems directly from considerations of how turbulence length scales behave in the logarithmic layer, and thus in other words the method is based solidly on physical reasoning. To be applicable to separated flows, the non-equilibrium effects are involved in the model, thus the model does not assume equilibrium boundary layer. Supersonic turbulent boundary layer on a flat plate at high Reynolds numbers are first used to verify the proposed model, and then the wall-modeled LES is applied to the shock-wave/turbulent boundary layer interacting separated flow at the higher Reynolds number (freestream Mach number of 1.69 and Reynolds number of $Re_\theta = 50,000$). The resulting method is shown to accurately predict equilibrium boundary layer at very high Reynolds numbers, with both realistic instantaneous fields (without overly elongated unphysical near-wall structures) and accurate statistics (both skin friction and turbulence quantities). Careful validations on the non-equilibrium separated flows will be discussed at the presentation.

Keywords: large-eddy simulation, wall modeling, high Reynolds number flow, separated flow.

1 Introduction

The promise of large eddy simulation (LES) is that it constitutes a more-or-less optimal compromise between predictive accuracy and computational cost. The energetic, dynamically important and flow-dependent motions are solved directly, leaving only motions with small energy and supposedly universal behavior to be modeled; this leads to predictive accuracy. Moreover, the computational cost is independent of the Reynolds number Re, since changes in Re only affect the spectrum at the smallest scales.

This favorable picture of LES is true in many situations, but changes completely when LES is applied to turbulent boundary layers. Boundary layers are multi-scale phenomena where the energetic and dynamically important motions in the inner layer (say, the innermost 10% of the boundary layer) become progressively smaller as the Reynolds number is increased. For the case of computing the flow over an airfoil, Chapman[1] estimated the required number of grid points as $N_{\rm total} \sim Re_c^{1.8}$, where Re_c is the chord Reynolds number. This is close to the cost of direct numerical simulation (DNS), and effectively prevents LES from being used on wall-bounded flows at realistic (high) Reynolds numbers for the foreseeable future.

The solution to this "near-wall problem" has been clear for a long time: the inner layer must be modeled rather than resolved[2, 3]. When directly resolving only the outer layer, Chapman[1] estimated a drastically lower $N_{\rm total} \sim Re_c^{0.4}$ for his airfoil example. There have been many proposed methods for modeling of the inner layer in LES (cf. the reviews by Piomelli and Balaras[4] and Spalart[5]). These wall-modeled LES approaches generally fall into one of two categories: 1) methods that model the wall shear stress τ_w directly, and 2) methods that switch to a Reynolds-averaged Navier-Stokes (RANS) description in the inner layer. The second category includes hybrid LES/RANS and detached eddy simulation (DES).

The hybrid LES/RANS and DES methods have become rather popular and are widely used with some success. These approaches blend a RANS-type turbulent eddy viscosity $\mu_{t,\rm RANS}$ near the wall with a LES-type subgrid-scale eddy viscosity $\mu_{t,\rm LES}$ away from the wall using a single mesh. Nikitin *et al.*[6] used DES as a wall-model with the switching location from RANS to LES placed in the logarithmic layer. For a range of different numerical methods and grid resolutions, they found a robust artificial "DES buffer layer" with an associated log-layer mismatch in the mean velocity profile (equivalent to about 15% underprediction of the skin friction). It was found that, near the switching location, the modeled contribution to the mean shear stress was too low while energy-carrying eddies had not yet been generated[7]. Therefore, in the hybrid LES/RANS and DES approaches, it is necessary to somehow stimulate instabilities and boost the resolved Reynolds stress near the LES/RANS interface to remove the log-layer mismatch. Piomelli *et al.*[7] used stochastic forcing and Shur *et al.*[8] proposed an empirically blended length scale that leads to a steep drop in the resultant eddy viscosity. Although these methods both energize the flow near the interface and improve the log-layer mismatch, they are to a certain extent empirical in nature. For example, when using stochastic forcing, Larsson *et al.*[9] found that the amplitude of the forcing could be adjusted to give a range of log-law intercepts. We also note that many recent improvements of DES include empirical functions with several parameters[5, 7, 8] that make the method more complicated.

The approach of modeling the wall shear stress τ_w directly is different from the hybrid LES/RANS and DES approaches. In the wall-stress-modeling approach, while the LES resolves only the outer layer, the LES is formally defined all the way down to the wall. A wall-model provides the instantaneous τ_w (needed by the LES as a boundary condition) given the instantaneous velocity field u_i at some distance h_{wm} off the wall (generally taken as the first grid point). Most wall-stress-modeling methods then use some form of RANS equations to estimate τ_w given $u_i(h_{\mathrm{wm}})$. Deardorff[2] and Schumann[3] introduced wall-stress-modeling by essentially imposing the log-law for the velocity at the first off-wall grid point. Grotzbach[10] later modified the Schumann-approach to instead inverting the log-law to provide τ_w for a given $u(y_1)$ (where subscript 1 denotes the first off-wall grid point). Balaras *et al.*[11] and Cabot and Moin[12] solved simplified RANS equations, based on the thin boundary-layer approximation with a mixing-length model, between the first grid point (at y_1) and the wall on an auxiliary grid refined only in the wall-normal direction. Compared to using the log-law, this includes effects of convection and pressure-gradient in the wall-model. Based on the fact that improved solutions were obtained when the mixing-length eddy viscosity was lowered from the standard RANS value[12], later Wang and Moin[13] proposed a dynamic procedure to determine the suitable model coefficient for the RANS mixing-length eddy viscosity model. This was then tested at a low Reynolds number ($Re_\theta = 3380$ where wall-resolved LES is accessible) with relatively fine mesh resolution. The grid used in the full wall-resolved LES (1536×96×42, $\Delta x^+ \approx 62$, $\Delta y^+ \approx 2$, $\Delta z^+ \approx 55$) was coarsened by approximately half in each direction (first grid point at $y^+ \approx 30$) and used for the wall-modeled LES mesh (768×64×24). These approximate wall-boundary-condition approaches have shown reasonable results with smaller log-layer mismatch than is typical in DES. However, these approaches have been mainly investigated in incompressible flows, with little work done for compressible flows. We also note that the dynamic procedure by Wang and Moin[13] has been tested only on at a single low Reynolds number.

The purpose of the present study is to address the error in the wall-stress-modeling approach and establish the wall-modeling for LES of high Reynolds number separated flows. After analyzing the source of the errors, we propose a simple yet effective dynamic wall-model to remove the error. The analysis and developments are presented for compressible flows, but everything extends trivially to incompressible flows. The resulting wall-model is validated against the corresponding experiments of shock-wave/turbulent boundary layer interaction by Souverein *et al.*[14, 15, 16]. The results are first validated on the undisturbed supersonic turbulent boundary layer at high Reynolds number: Mach 1.69 and $Re_\delta = 6.1 \times 10^5$ based on the boundary layer thickness (momentum thickness based $Re_\theta = 5 \times 10^4$), and then the non-equilibrium wall-model is applied to the shock-wave/turbulent boundary layer interacting flow at the same Mach number and Reynolds number. The results from the wall-modeled LES are compared to the corresponding experiments by Souverein *et al.*[14, 15, 16].

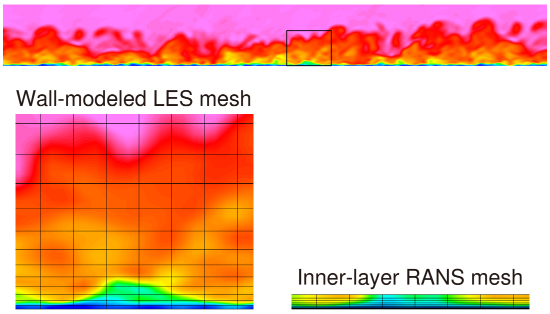

Figure 1: Sample of meshes for wall-modeled LES. LES-grid based on outer length scales only (left) and auxiliary RANS-grid in inner layer for estimation of the wall shear stress.

2 Wall-modeled LES framework

The proposed wall-model is based on the wall-stress-modeling approach. The LES mesh is designed to resolve only the outer-layer large scales (thus the grid resolution scales with the boundary layer thickness δ) and does not resolve the viscous sublayer. The wall shear stress τ_w is computed through solving RANS equations on an auxiliary grid in the inner layer. This grid is embedded in the LES mesh and refined in the wall-normal direction only, as illustrated in Fig. 1. Since compressible flow is considered here, the auxiliary RANS also provides the wall heat flux to the LES. The RANS is forced at its top boundary by the instantaneous solution in the LES at the corresponding point. The matching location $h_{\rm wm}$ in the LES mesh where the RANS top boundary matches to the LES mesh is not necessarily taken at the first off-wall LES point, as has been the case in all prior studies that the author is aware of. To allow for the forcing errors due to the subgrid modeling and numerics to be made arbitrarily small, based on our study[17] fifth grid point off the wall ($h_{\rm wm} = 0.055y/\delta$ and $y^+ \approx 878$) in the LES mesh is matched to the RANS top boundary in this study. We note that although the inner-layer RANS mesh is embedded in the wall-modeled LES mesh, the information given from the RANS to LES is only through the wall shear stress and heat flux, while the information from the LES to RANS is solely through the forcing at the top boundary of the RANS.

2.1 Evolution equations and numerical method

The evolution equations in the LES and the auxiliary RANS are the compressible filtered or ensemble-averaged Navier-Stokes equations for a perfect gas and are identical except for the boundary conditions and the values of the model constants for the residual stresses and heat fluxes.

The spatial discretization is fully conservative and uses a sixth-order compact differencing scheme[18], with some modifications made necessary by the wall-modeling; these modifications are discussed below. Aliasing errors are contained by applying an eighth-order low-pass spatial filter to the conserved variables at regular intervals. Time-integration is done by a classic four-stage, fourth-order explicit Runge-Kutta method on the LES grid. To alleviate a severe CFL time-step restriction in the inner-layer RANS computation due to the highly refined mesh in wall-normal direction, a second-order fully implicit time-integration scheme[19, 20] is used there. Three steps of sub-iterations (Newton-Raphson iteration) are adopted to minimize the errors due to the linearization in the implicit scheme. The code has been extensively verified and validated[21, 22, 23, 24].

The computational domain for the wall-modeled LES is $15\delta_r$, $15\delta_r$ and $3\delta_r$ in streamwise (x), wall-normal (y) and spanwise (z) directions where δ_r is a reference boundary layer thickness that is close to its value at the inlet. The wall is located at $y = 0$, and the corresponding grid index is 0; hence $y_0 = y_w = 0$. The boundary layer thickness δ at the station where statistics are compared is $\delta \approx 1.2\delta_r$ ($x/\delta_r \approx 12$). A buffer layer with the length of $12\delta_r$ is placed at the upper boundary to remove turbulent fluctuations and any reflections from the boundary. The horizontal (wall-parallel plane) mesh distributions for the inner-layer RANS mesh are the same as the outer-layer LES mesh, while the RANS mesh is significantly refined in the wall-normal direction (y^+ at the first grid point off the wall is less than 1) to resolve the viscous sublayer in a RANS sense. We note that no complex procedure is necessary to generate the inner-layer RANS mesh since only wall-normal refinement is required, which can be easily done within the preprocessing of the simulation. The rescaling-reintroducing method of Urbin and Knight[25] is used to produce realistic turbulence at the inflow for both the inner-layer RANS and outer-layer LES, with the recycling station taken as $12\delta_r$ downstream of the inflow.

2.2 LES: Subgrid Model and Boundary Conditions

The dynamic Smagorinsky model of Moin *et al.*[26] with the modification of Lilly[27] is used to calculate the turbulent eddy viscosity μ_t and turbulent Prandtl number Pr_t.

The LES equations requires boundary conditions at the wall, specifically the convective and viscous fluxes. At walls, the kinematic no-penetration condition implies that the convective terms are zero. In addition, the viscous work term $\tau_{ij}u_i$ is zero at the wall due to the no-slip condition (the fact that the LES does not resolve the inner layer does not change the fact that $u_i = 0$ at a wall, only that the gradient can not be computed accurately). Since the first grid point in the LES is above the viscous inner layer (i.e., $y_1^+ > 50$), we can not estimate the wall shear stress directly from the information in the LES; thus τ_w and the wall heat flux q_w are taken from the auxiliary RANS wall-model as boundary conditions.

The fact that the viscous inner layer is not resolved implies that some changes are needed in the numerical method as well. Simply put, differentiation and filtering between points above and below this missing inner layer (i.e., between the first grid point $j = 1$ and the wall) are ill-defined and not accurate. We instead compute wall-normal derivatives at $j = 1$ using a completely one-sided formula and at $j = 2$ using a second-order central formula; remaining grid points are treated by the tri-diagonal compact scheme. Although, given these numerical treatments, the LES equations can be evaluated without specifying the velocities, density and temperature at the wall, we use slip-wall conditions with extrapolation from the interior nodes to calculate the dynamic Smagorinsky model and for low-pass spatial filtering.

2.3 Auxiliary RANS: Turbulence Model and Simplified Formulation

A simple mixing-length eddy-viscosity model with near-wall damping is used to determine the μ_t in the inner-layer RANS as

$$\mu_t = \kappa_{\mathrm{mod}} \rho y \sqrt{\frac{\tau_w}{\rho}} \mathcal{D} \ , \quad \mathcal{D} = \left[1 - \exp(-y^+/A^+)\right]^2 \ , \tag{1}$$

where $y^+ = \rho_w y u_\tau / \mu_w$ is the wall-distance in viscous units, and we note that $\sqrt{\tau_w/\rho}$ is the velocity scale in a boundary layer with varying mean density. The model parameter A^+ is taken as 17 throughout this work. The model parameter κ_{mod} is either determined through the dynamic procedure as will be discussed in the following Section 3, or taken as equal to the von Kármán constant $\kappa = 0.41$. Similarly, the turbulent Prandtl number in Eq. 6 is either determined dynamically or taken as constant at 0.9.

The full wall-model is to solve the time-dependent full RANS equations on the auxiliary inner-layer RANS mesh, with non-slip adiabatic wall conditions and the solution at the top of the RANS mesh set equal to the instantaneous LES solution at the corresponding (matching) location every time step. Since the RANS mesh is resolved in the wall-normal direction, the resulting wall shear stress and wall heat flux (or, in the case of an isothermal wall, the wall temperature) can be computed.

In addition to this full wall-model, we also consider the simplified equilibrium boundary layer equations (which then replace the full RANS equations)

$$\frac{d}{dy}\left[(\mu + \mu_t)\frac{du}{dy}\right] = 0 \, , \tag{2}$$

$$\frac{d}{dy}\left[(\mu + \mu_t) u \frac{du}{dy} + \frac{1}{\gamma - 1}\left(\frac{\mu}{Pr} + \frac{\mu_t}{Pr_t}\right)\frac{dc_s^2}{dy}\right] = 0 \, , \tag{3}$$

which was derived from the conservation equations for streamwise momentum and total energy with use of the standard approximations in equilibrium boundary layer flow[28]. Since these simple equations are supposed to be accurate for zero-pressure-gradient equilibrium flows considered in the first test case, we can compare this simple model with the full wall-models to investigate the capability of the full wall-models.

Note that the pressure is constant in the wall-normal direction and simply imposed by the LES in the equilibrium model while the pressure is solved in the full RANS wall-model. The simplified equilibrium model 2–3 is a system of two coupled ODEs that are solved numerically on a temporary 1D grid in the present implementation (thus the 3D auxiliary RANS mesh is not needed). Note that, in the incompressible limit without heat transfer, the equilibrium wall-model is equivalent to the famous log-law in the inviscid region.

3 Errors in wall modeling

To close the system of time-dependent full RANS equations on the inner-layer mesh, one must set the two modeling constants $\kappa_{\rm mod}$ in Eq. 1 and Pr_t in the inner-layer RANS equations. The standard RANS value $\kappa_{\rm mod} = \kappa = 0.41$ (and $Pr_t \approx 0.9$ with heat transfer) was typically used in the earliest studies[11, 12]. However, as pointed out by Cabot and Moin[12], since the Reynolds stress carried by the nonlinear convective terms in the inner-layer RANS equations is significant near the matching location, the RANS eddy-viscosity must be reduced to account for only the unresolved components.

Based on the finding that improved solutions were obtained when the model constant $\kappa_{\rm mod}$ was lowered from the standard RANS value[12], Wang and Moin[13] introduced a dynamic procedure to adjust the model coefficient $\kappa_{\rm mod}$. The idea of Wang and Moin (when extended to compressible flow) is to match the total shear stress $-\overline{\rho}\widetilde{u''v''} + (\overline{\mu} + \overline{\mu_t})\partial\widetilde{u}/\partial y$ between the LES and RANS at the matching location. Since the velocity, density and temperature are given from the LES as a boundary condition for RANS, this means that the resolved portion is identical in LES and RANS at the matching location. If one further assumes that the velocity and temperature have the same slope in RANS and LES, the matching condition amounts to matching $\mu_{t,LES}$ and $\mu_{t,RANS}$ (and $Pr_{t,LES}$ and $Pr_{t,RANS}$ when extended to compressible flow). Wang and Moin[13] used this matching condition $\langle\mu_{t,RANS}\rangle = \langle\mu_{t,LES}\rangle$ (where $\langle\cdot\rangle$ was taken as the average in the spanwise direction and over the previous 150 time steps) to find the value of the parameter $\widehat{\kappa}$. The resulting reduced constant was then applied throughout the boundary layer in the inner-layer RANS simulation, i.e., they took $\kappa_{\rm mod} = \widehat{\kappa}$. This dynamic procedure was tested through the incompressible turbulent boundary layer flow past an airfoil trailing-edge at low Reynolds number ($Re_\theta = 3380$ where wall-resolved LES data was available), and they obtained improved results compared with using the typical constant value $\kappa_{\rm mod}$=0.41. However, we note that this dynamic procedure has been tested only on at the single low Reynolds number with the matching location $h_{\rm wm} = y_1$ where wall models suffer from the numerical and subgrid-modeling errors in near-wall grid points as discussed in Ref. [17]. It will be shown below that this dynamic procedure does not work at all at high Reynolds numbers when y_1^+ becomes large. Specifically, it will be shown that the crucial flaw is the use of $\kappa_{\rm mod} = \widehat{\kappa}$ through-out the inner RANS layer.

3.1 Proposed dynamic wall modeling

In this section, we propose a simple mesh-resolution-dependent dynamic procedure for compressible flows (that is trivially extendable to incompressible flows). Since the velocities and temperature are matched at the top of the inner-layer RANS, the resolved portion of the stresses and heat fluxes from the inner- and outer-layer calculations are the same. To match the total stresses and heat fluxes approximately at the matching location, the unresolved stresses and heat fluxes need to be matched. Similarly to the procedure of Wang and Moin[13], we approximately match the total stresses and heat fluxes at the matching location h_{wm} by matching the turbulent eddy viscosity and turbulent thermal conductivity ($C_p\mu_t/Pr_t$). We thus first find the value

$$\widehat{\kappa} = \frac{\langle \mu_{t,LES} \rangle}{\langle \rho y \sqrt{\frac{\tau_w}{\rho}} \mathcal{D} \rangle}, \tag{4}$$

that matches the RANS and LES eddy-viscosities at the matching location h_{wm}. The angular brackets denote averaging in the spanwise direction, and thus $\widehat{\kappa}$ is varying in the streamwise direction and time. We approximately match the turbulent conductivities by taking $\widehat{Pr}_{t,RANS} = \langle Pr_{t,LES} \rangle$.

The objective of the proposed mesh-resolution-dependent (wall-normal-dependent) dynamic procedure is to approximately account for the fact that the division between resolved and unresolved stresses changes dramatically in the wall-normal direction in the near-wall RANS, partly due to the exceedingly anisotropic mesh used at high Reynolds number for the RANS. The size of the energetic and stress-carrying motions in the log-layer is proportional to the wall-distance y[28]. We take $L_{\|} = C_{\|} y$ as a characteristic length scale of the energetic and stress-carrying motions within the log-layer, where $C_{\|}$ is a constant and is dictated by flow physics, specifically the structure of the energetic motions in the log-layer. The subscript $\|$ implies that the length scale is in the wall-parallel directions, so some combination of the L_x and L_z. Let us introduce the ratio of the length scale to the wall-parallel grid spacing $L_{\|}/\Delta_{\|} = C_{\|} y/\Delta_{\|}$, where $\Delta_{\|} = \max(\Delta x, \Delta z)$. In practice the grid for the outer-layer LES may be nearly isotropic, and thus the impact of this specific choice is not considered to be crucial. We also note that the numerical tests were performed with two different meshes ($\Delta x = \Delta z$ and $\Delta x = 5/3\Delta z$) with the same conclusions (see Ref. [29] for details of $\Delta x = 5/3\Delta z$ case). The scale of $\Delta_{\|}$ can be considered as approximately equivalent to the smallest eddy size that the mesh can possibly support, and thus $L_{\|}/\Delta_{\|}$ is considered to be the critical parameter in the wall-parallel direction. If $L_{\|}/\Delta_{\|}$ is smaller than some constant α where the value of α (i.e., the number of grid points per wavelength) depends on the numerical method used for the inner-layer RANS, we may assume that the resolved stress is negligibly small. Thus typical RANS constants, $\kappa_{\mathrm{mod}} = 0.41$ and $Pr_t = 0.9$, should be used. If $L_{\|}/\Delta_{\|} > \alpha$, the constants should be reduced towards the adjusted constants at the matching location. We note that since the RANS mesh is significantly refined in the wall-normal direction to resolve the viscous layer in the RANS sense, Δy is fine enough to resolve L_y and also $\Delta y < \Delta_{\|}$. In this study, we use a linear damping function $\mathcal{K}$ to define

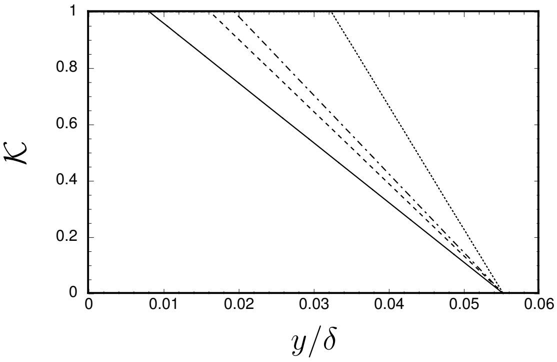

Figure 2: Linear blending function $\mathcal{K}$ with $\alpha' = 0.2$ (solid line), $\alpha' = 0.4$ (dashed line), $\alpha' = 0.48$ (dashed-dotted line), and $\alpha' = 0.8$ (dotted line).

$$\kappa_{\text{mod}} = 0.41\mathcal{K} + \widehat{\kappa}(1-\mathcal{K})\,, \tag{5}$$
$$Pr_t = 0.9\mathcal{K} + \widehat{Pr}_t(1-\mathcal{K})\,, \tag{6}$$

where

$$\mathcal{K} = \min\left\{\frac{L_{\|,h_{\text{wm}}}/\Delta_\| - L_\|/\Delta_\|}{L_{\|,h_{\text{wm}}}/\Delta_\| - \alpha}\ ,\ 1\right\}$$

or equivalently

$$\mathcal{K} = \min\left\{\frac{h_{\text{wm}} - y}{h_{\text{wm}} - y_{\text{crit}}}\ ,\ 1\right\}\ ,\quad y_{\text{crit}} = \frac{\alpha}{C_\|}\Delta_\| = \alpha'\Delta_\|\,. \tag{7}$$

The latter form 7 makes it clear that $\mathcal{K}$ is only a function of y and the parameter $\alpha' = \alpha/C_\|$, with h_{wm} and $\Delta_\|$ being determined by the grid. Specifically, note that $\mathcal{K}$ is not flow-dependent. Figure 2 shows the linear damping function $\mathcal{K}$ with different constants α'. We first show the results by fixing $\alpha' = 0.48$, and then address the sensitivity of the flow statistics to this parameter.

4 Results

In this section we compare the dynamic procedure proposed above with the wall-normal independent dynamic-coefficient approach by Wang and Moin[13] ($\kappa_{\text{mod}} = \widehat{\kappa}$ and $Pr_t = \widehat{Pr}_{t,RANS}$). We also compare to the constant-coefficient approach ($\kappa_{\text{mod}} = 0.41$ and $Pr_t = 0.9$) and equilibrium wall-model approach (solving ODEs 2–3).

The flow condition considered in this study is based on the experiments of high Reynolds number supersonic turbulent boundary layer on a flat plate and shock-wave/turbulent boundary layer interaction performed by Souverein *et al.* [14, 15]. In both the cases, the freestream Mach number is 1.69 and the Reynolds number is $Re_\delta = 6.1 \times 10^5$

($Re_\theta = 5 \times 10^3$). The results are first validated on the undisturbed supersonic turbulent boundary layer and then the non-equilibrium wall-model is applied to the shock-wave/turbulent boundary layer interacting flow. The results from the wall-modeled LES are compared to the corresponding experiments by Souverein *et al.*[14, 15, 16], the incompressible experiments by DeGraaff and Eaton[30] at high Reynolds numbers, the DNS by Pirozzoli and Bernardini[31], and finally to wall-resolved LES at low Reynolds number. We again emphasize that this is a *much* higher Reynolds number than what wall-resolved LES or DNS can reach.

The grid resolution in the wall-parallel directions is held constant at $\Delta x = \Delta z \approx 0.042\delta$ for all simulations, while varying the near-wall wall-normal grid resolution. In the wall-normal direction, an approximately uniformly spaced grid ($\Delta y_w = 0.011\delta$) is used below the matching location (fifth grid point off the wall $h_{\rm wm} = y_5$ in this study). The grid is smoothly stretched in the region $h_{\rm wm} \leq y \leq 1.4\delta_r$, and then keeps a uniformly spaced grid $\Delta y \approx 0.025\delta$ from $y = 1.4$ to $3\delta_r$ In viscous wall units, $\Delta x^+ = \Delta z^+ \approx 640$, and the equally spaced $\Delta y^+ \approx 385$; hence the grid spacing is *much* coarser than in traditional wall-resolved LES.

Four different inner-layer RANS models are considered:

1. EQBL: equilibrium wall-model (solving ODEs 2–3),
2. CNST: full RANS + constant coefficients ($\kappa_{\rm mod}$=0.41 and Pr_t=0.9),
3. CDYN: full RANS + y-constant dynamic approach ($\kappa_{\rm mod} = \widehat{\kappa}$ and $Pr_t = \widehat{Pr}_{t,RANS}$),
4. VDYN: full RANS + y-variable dynamic approach (Eqs. 5 and 6).

4.1 Undisturbed supersonic turbulent boundary layer

4.1.1 Mean and fluctuation statistics

Figure 3 shows the mean streamwise velocity profiles where the computed results are compared with the log-law and experiments[14, 15, 30]. The VDYN result is almost identical to the EQBL result and in good agreement with the experiments and the log-law. The logarithmic region appears clearly for $y^+ < 3000$ without showing the logarithmic layer mismatch. Although the slope of the logarithmic region is well predicted in CNST, the CNST result shows a lower intercept, indicating higher skin friction (7% higher than EQBL). This trend is consistent with the findings of Cabot and Moin[12] and Wang and Moin[13]. CDYN is the wall-normal-independent dynamic-coefficient approach and essentially the choice of Wang and Moin[13]. Although the total stress is approximately matched at the RANS top boundary, the y-constant dynamic procedure reduces the value of $\kappa_{\rm mod}$ with a constant factor of approximately 1/50 at this high Reynolds number flow throughout the inner-layer and laminarizes the inner-layer flow, resulting in an intercept of approximately 65 (much too low wall shear stress, approximately 1/6 of EQBL).

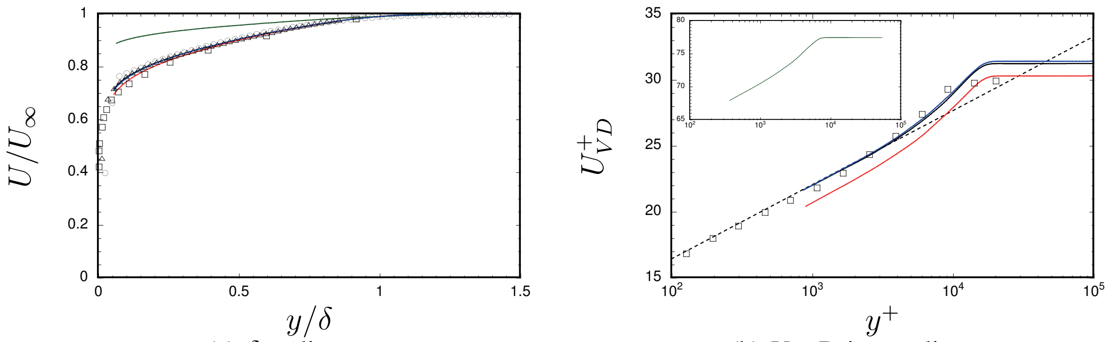

(a) δ scaling.
(b) Van Driest scaling.

Figure 3: Mean streamwise velocity: δ scaling (left) and Van Driest scaling (right). EQBL (black); CNST (red); CDYN (green, visible only in insert in figure b); VDYN with $\alpha' = 0.48$ (blue); the log-law $\ln(y^+)/0.41 + 5.2$ (dashed line); corresponding experiments[14, 15], dual-PIV (circles), high-resolution zoom-PIV(triangles); incompressible experiments at $Re_\theta = 31,000$ (squares)[30].

This is also evident in the mean eddy viscosity profiles for the four different inner-layer RANS models as shown in Fig. 4. The CDYN approach reduces the eddy viscosity significantly throughout the inner layer, with $\overline{\mu_t}/\mu \lesssim 4$. On the other hand, the VDYN approach maintains the original RANS eddy viscosity up to $y = \alpha'\Delta_{\parallel}$ as designed and gradually reduces μ_t toward the matching location where the total stress between inner and outer layer is approximately matched. The results indicate that the unresolved stresses and heat fluxes are increased in the wall-normal direction from the matching location toward the wall in the RANS mesh and this physics must be properly modeled. The proposed y-variable dynamic approach (VDYN) that approximately accounts for this physics is shown to be superior to the other models. The successful results obtained by the y-constant dynamic procedure by Wang and Moin[13] for their case was probably due to the low Reynolds number ($Re_\theta = 3380$) in their study, coupled with them having the matching location near the buffer layer at $h^+_{\mathrm{wm}} \approx 30$.

Resolved Reynolds normal stresses and shear stress are plotted in Fig. 5 with the experimental data[14, 15, 30] and low Reynolds number DNS[31]. EQBL, CNST and VDYN show almost identical results with minor differences and reasonable agreement with the experimental data and DNS data. Only the CDYN results behave differently. This is primarily because of the too-low wall shear stress (approximately 1/6 of EQBL) given by the CDYN wall-model, resulting in the lower resolved Reynolds stresses. Note that the $\overline{\tau_w}$ normalization used in Fig. 5 (the value of $\overline{\tau_w}$ is different in each wall-model, i.e., $\overline{\tau_w}_{CDYN} \approx 1/6\overline{\tau_w}_{EQBL}$) causes the higher values of CDYN, although the actual fluctuations obtained by CDYN are smaller than the others. It is worth noting the uncertainty involved in the corresponding experiments[14, 15]. As noted in [15], the experimental velocity fluctuations include a contribution from the measurement noise, and the noise likely causes the slight overestimation of the u-fluctuations. The underestimation of the v-fluctuations is a measurement artifact, re-

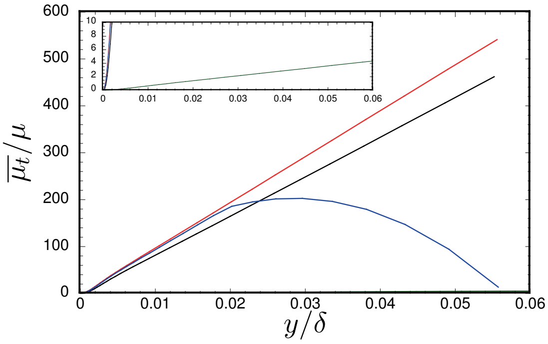

Figure 4: Mean turbulent eddy viscosity in inner-layer RANS. EQBL (black); CNST (red); CDYN (green, visible in insert only); VDYN with $\alpha' = 0.48$ (blue).

lated to the dynamic range of the measurement system and the measurement settings. By consequence, the under-resolved v-fluctuations lead to underestimated Reynolds shear stress values, particularly below $y/\delta = 0.3$.

Figure 6 shows mean and fluctuation temperature and density profiles. Since there is no available thermodynamic data at this Mach number, we computed wall-resolved LES at Mach 1.69 and $Re_\theta \approx 2,200$ and compare to the wall-modeled LES. A brief description of the wall-resolved LES is that the employed grid resolutions are $\Delta x^+ = 24$, $\Delta y^+ = 0.64 - 24$ and $\Delta z^+ = 12$, and the sixth-order compact differencing scheme with RK4 method is used. We note that the Van Driest transformed mean velocity and resolved stresses in Morkovin scaling obtained by the wall-resolved LES shows excellent agreements with the DNS at Mach 2.28 and $Re_\theta \approx 2,300$ by Pirozzoli and Bernardini[31]. EQBL, CNST and VDYN again show almost identical results and the computed mean thermodynamic quantities closely agree with the wall-resolved LES, whereas the thermodynamic fluctuations are underpredicted by approximately 20%. CDYN completely underpredicts the mean and fluctuation of the thermodynamic quantities throughout the boundary layer.

The results have shown how the computed statistics, especially the skin friction, are improved by employing the proposed dynamic wall-model. We next show that the method yields physically realistic turbulence near the wall. Figure 7 shows contours of the instantaneous streamwise velocity fluctuations in a wall-parallel plane at the matching location (within the logarithmic region at $y^+ = 878$) obtained by the wall-modeled LES with the y-variable dynamic approach (VDYN). The wall-modeled LES does not produce smooth nearly one-dimensional unphysical eddies as commonly seen in hybrid LES/RANS and standard DES methods[4].

4.1.2 Sensitivity to the free parameter α'

We have shown that the proposed dynamic wall-model improves the computed statistics (i.e., reducing the errors in wall-modeling), especially the skin friction, at the high Reynolds number with the only adjustable parameter in the model at $\alpha' = 0.48$. The

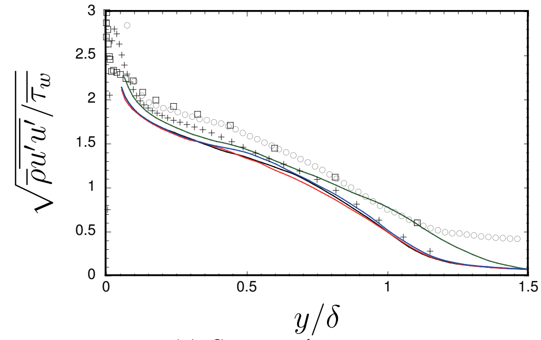

(a) Streamwise stress.

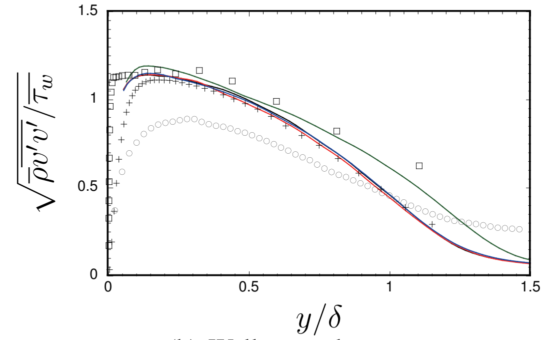

(b) Wall-normal stress.

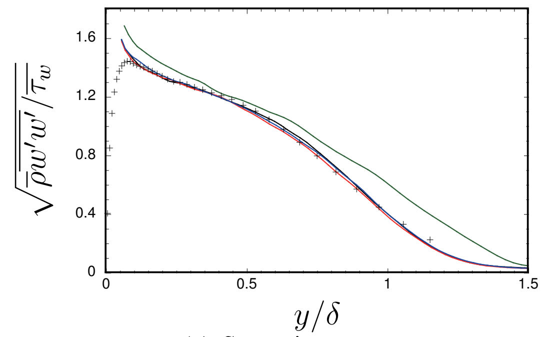

(c) Spanwise stress.

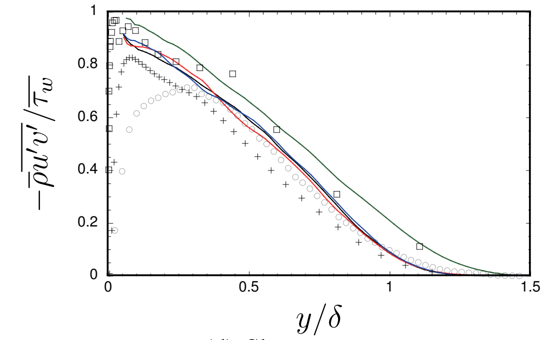

(d) Shear stress.

Figure 5: Resolved Reynolds normal stresses and shear stress. EQBL (black); CNST (red); CDYN (green); VDYN with $\alpha' = 0.48$ (blue); corresponding experiments[14, 15] (circles); incompressible experiments at $Re_\theta = 13,000$ (squares)[30]; DNS at Mach 2.28 and $Re_\theta \approx 2,300$ (pluses)[31].

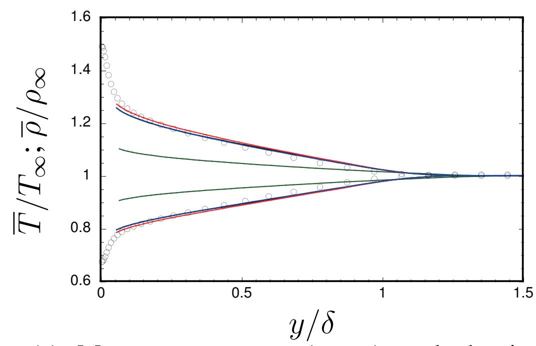

(a) Mean temperature (upper) and density (lower).

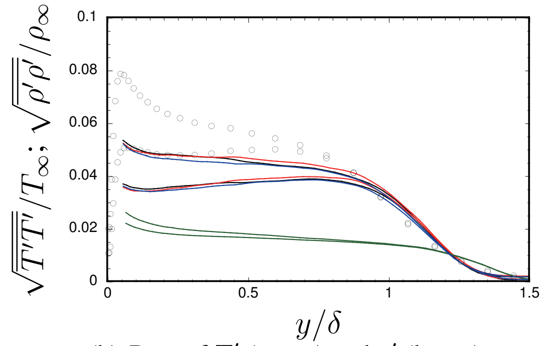

(b) Rms of T' (upper) and ρ' (lower).

Figure 6: Mean (left) and fluctuation (right) of temperature and density compared to wall-resolved LES at Mach 1.69 and $Re_\theta \approx 2,200$ (circles). EQBL (black); CNST (red); CDYN (green); VDYN with $\alpha' = 0.48$ (blue).

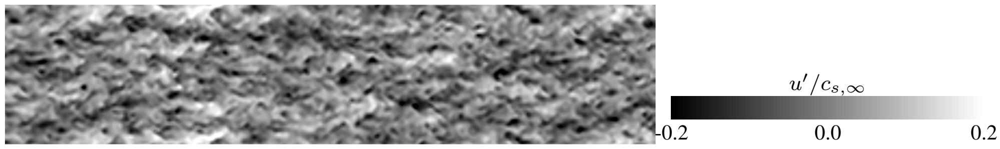

Figure 7: Instantaneous streamwise velocity fluctuation in wall parallel plane at matching location (logarithmic region at $y^+ = 878$) obtained by VDYN with $\alpha' = 0.48$.

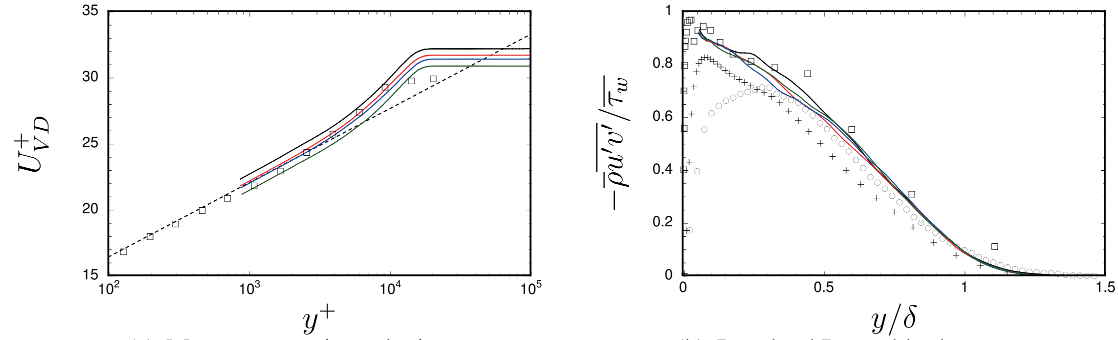

(a) Mean streamwise velocity. (b) Resolved Reynolds shear stress.

Figure 8: Mean streamwise velocity (van Driest-transformed) and Resolved Reynolds shear stress at $Re_\theta = 50,000$ obtained by VDYN method with $\alpha' = 0.2$ (black), $\alpha' = 0.4$ (red), $\alpha' = 0.48$ (blue), and $\alpha' = 0.8$ (green). Compared to the log-law $\ln(y^+)/0.41 + 5.2$ (dashed line); incompressible experiments at $Re_\theta = 31,000$ (squares)[30]; corresponding experiments[14, 15] (circles); DNS at Mach 2.28 and $Re_\theta \approx 2,300$ (pluses)[31].

value of α' controls the location where the original RANS eddy viscosity and turbulent Prandtl number start blending with the adjusted constants at the matching location. If the results are too sensitive to this value, the applicability of the proposed model might be reduced. Here we address this issue by investigating the sensitivity of flow statistics to α'.

The sensitivity of the flow statistics to α' at $Re_\theta = 50,000$ in the y-variable dynamic approach is shown in Fig. 8. The choices of $\alpha' = 0.2$, 0.4, 0.48 and 0.8 start blending the eddy viscosity and turbulent Prandtl number at 15, 32, 36 and 60 % of the inner-layer RANS, respectively (see Fig. 2). It is clear that the results are largely insensitive to the choice of α', and with the current numerical schemes the choice of $\alpha' = 0.48$ was found to yield the best fit to the log-law. The wall shear stress is slightly underestimated by 4.3% with $\alpha' = 0.2$ and overestimated by 3.3% with $\alpha' = 0.8$ respectively when compared to the corresponding EQBL result. Although not shown here, resolved Reynolds normal stresses and thermodynamic quantities are also insensitive to α'. We note that the optimal value of α' naturally depends on the numerics used for the inner-layer RANS simulation, but this sensitivity study suggests that the impact on the computed statistics is small.

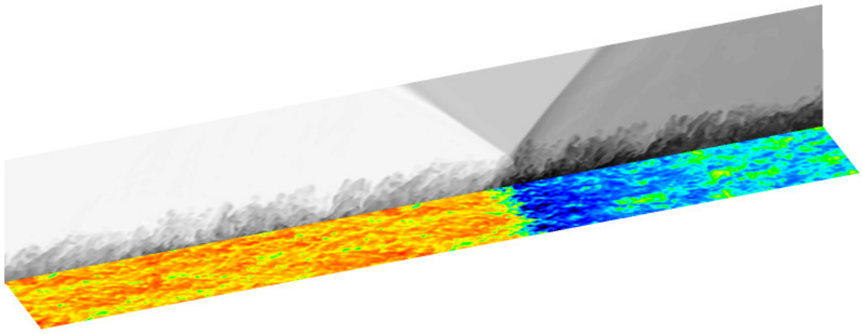

Figure 9: Wall-modeled LES of shock/turbulent boundary layer interaction at $M_\infty = 1.69$ and $Re_\delta = 6.1 \times 10^5$ ($Re_\theta = 5 \times 10^4$). Streamwise velocity contours at wall-parallel plane at $y = h_{\rm wm}$ ($h^+_{\rm wm} \approx 590$) and temperature contours at side-plane.

4.2 Shock-wave/turbulent boundary layer interaction

Having verified the proposed dynamic method on the turbulent boundary layer that essentially removes the impact of the wall-modeling errors on the computed statistics, we next discuss the capability of the established wall-model on non-equilibrium separated flows. We consider the shock-induced separated turbulent boundary layers at $M_\infty = 1.69$, $Re_\delta = 6.1 \times 10^5$ ($Re_\theta = 5 \times 10^4$), and flow deflection angle by the oblique shock $\beta = 6.0$, which is experimentally performed by Souverein *et al.* [14, 15]. Here again, we stress that this is a *much* higher Reynolds number than what traditional wall-resolved LES is capable. The grid used here corresponds to the $h_{\rm wm} = y_5 = 0.055y/\delta$ grid ($\Delta x = \Delta z \approx 0.042\delta$ and $\Delta y_w/\delta = 0.011$) used in previous Section 44.1. This configuration was shown in that section to yield converged statistics. The localized artificial diffusivity method [23] is used to capture the shock waves coupled with the sixth-order compact differencing scheme.

Figure 9 shows the instantaneous snapshot of the wall-modeled LES of the shock wave/turbulent boundary interaction. We conduct concurrent simulations of a supersonic turbulent boundary layer that are coupled with the shock interaction computation. The inflow conditions for the wall-modeled LES of shock-wave/boundary layer interaction are extracted from the plane of concurrent wall-modeled LES of supersonic turbulent boundary layer. Typical low-speed streaks (orange colored regions) in the upstream of the shock interaction and instantaneous reverse flow regions (blue colored regions) in the shock-induced separating region are clearly observed in the wall-parallel plane.

Comparisons of mean and variance of streamwise velocity in the region of shock-interacting separated flow between the wall-modeled LES and experiment are shown in Fig. 10. Overall the locations of the shock structures, boundary layer separation, thickening of the turbulent boundary layer after the shock interaction, and the high fluctuation u' region along the separated boundary layer qualitatively agree reasonably well with the experiment. However, quantitatively, the wall-modeled LES under-

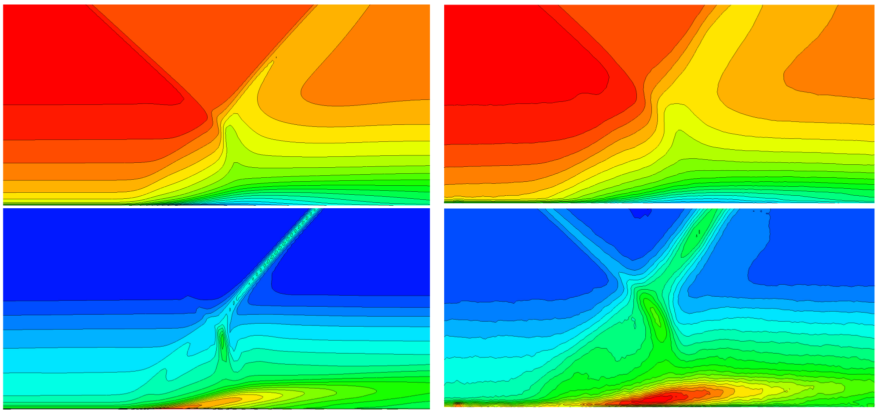

(a) Wall-modeled LES (b) Experiment

Figure 10: Comparisons of mean streamwise velocity (top) and streamwise velocity fluctuation (bottom) distributions between wall-modeled LES and experiment[14, 15]. Region of $-3.1 \lesssim (x - x_s)/\delta_0 \lesssim 1.15$ and $0 \lesssim y/\delta_0 \lesssim 2$ (x_s is the inviscid shock impingement point). 20 equally spaced contours: $-0.1 \leq U/U_\infty \leq 0.99$, $0 \leq u'/U_\infty \leq 0.18$.

predicts the peak u' in the separated region. Mesh convergence study using multiple meshes and more detailed comparisons between the wall-modeled LES and the experimental data in the mean and fluctuation quantities will be given at the presentation. Significant improvements are expected to come from refinements of the grid, especially at the shock-induced separated region where fine-scale vortices are generated along the separated shear layer.

5 Summary

This paper addresses the errors encountered when modeling the wall shear stress (and heat flux when extended to compressible flow) in large-eddy simulation (LES) on grids that do not resolve the viscous layer: the errors in estimating the wall shear stress from a given outer-layer velocity.

We propose a simple yet efficient dynamic wall-model that minimize the impact of the error on the computed statistics (most importantly, the predicted skin friction) and make the wall-model applicable at high Reynolds numbers. The model stems directly from considerations of how turbulence length scales behave in the logarithmic layer, and thus in other words the method is based solidly on physical reasoning. Supersonic turbulent boundary layer on a flat plate at high Reynolds number, Mach 1.69 and $Re_\delta = 6.1 \times 10^5$ ($Re_\theta = 5 \times 10^4$), is simulated and compared with the available experimental and DNS/LES data. We note that the wall-model and the arguments leading to the proposed method are presented for compressible flows, but everything extends trivially to incompressible flows.

We proposed a mesh-resolution-dependent (y-variable) dynamic wall-model to address the wall-modeling errors. The wall-model approximately matches the total stresses and heat fluxes at the matching location and also accounts for the physics that the unresolved stresses and heat fluxes are increased in the wall-normal direction toward the wall in the inner-layer RANS. The model has only one adjustable parameter α', the value of which is shown to have only a small effect on the results. The proposed dynamic wall-model shows good agreement with the available experimental and DNS/LES data on the flat plate supersonic turbulent boundary layer case without showing the typical logarithmic layer mismatch, whereas no existing wall-stress models that solve the RANS equations on the embedded inner-layer mesh without a control theory were able to predict the correct intercept in the Van Driest transformed velocity (i.e., the skin friction). The method also produces realistic near-wall turbulence without the overly smooth and elongated "streaks" common to several other approaches.

Finally the established wall model is tested on the shock-wave/turbulent boundary layer interacting separated flow at the higher Reynolds number. Preliminary results show a qualitatively reasonable agreement with the experimental data, although the velocity fluctuation in the separated region is underpredicted. Careful mesh refinement and validation studies on this non-equilibrium separated flows will be discussed at the presentation.

Acknowledgments

This work was supported in part by the JAXA International Top Young Fellowship Program, and Grant-in-Aid for Young Scientists (B) KAKENHI 24760670. Computer time was provided by Japan Aerospace Exploration Agency (JAXA) Supercomputer System at JAXA. The authors gratefully acknowledge Dr. Louis J. Souverein and Professor Sergio Pirozzoli for providing extensive experimental and DNS data. The authors are also grateful to Professor Sanjiva K. Lele for valuable discussions.

References

[1] D.R. Chapman, "Computational Aerodynamics Development and Outlook", *AIAA Journal*, 17(12): 1293–1313, December 1979.

[2] J.W. Deardorff, "A Numerical Study of Three-Dimensional Turbulent Channel Flow at Large Reynolds Number", *Journal of Fluid Mechanics*, 41: 453–480, 1970.

[3] U. Schumann, "Subgrid Scale Model for Finite Difference Simulations of Turbulent Flows in Plane Channels and Annuli", *Journal of Computational Physics*, 18(4): 376–404, 1975.

[4] U. Piomelli, E. Balaras, "Wall-Layer Models for Large-Eddy Simulations", *Annual Review of Fluid Mechanics*, 34: 349–374, 2002.

[5] P.R. Spalart, "Detached-Eddy Simulation", *Annual Review of Fluid Mechanics*, 41: 181–202, 2009.
[6] N.V. Nikitin, F. Nicoud, B. Wasistho, K.D. Squires, P.R. Spalart, "An Approach to Wall Modeling in Large-Eddy Simulations", *Physics of Fluids*, 12(7): 1629–1632, July 2000.
[7] U. Piomelli, E. Balaras, H. Pasinato, K.D. Squires, P.R. Spalart, "The Inner-Outer Layer Interface in Large-Eddy Simulations with Wall-Layer Models", *International Journal of Heat and Fluid Flow*, 24(4): 538–550, August 2003.
[8] M.L. Shur, P.R. Spalart, M.K. Strelets, A.K. Travin, "A Hybrid RANS-LES Approach with Delayed-DES and Wall-Modelled LES Capabilities", *International Journal of Heat and Fluid Flow*, 29(6): 1638–1649, December 2008.
[9] J. Larsson, F.S. Lien, E. Yee, "Feedback-Controlled Forcing in Hybrid LES/RANS", *International Journal of Computational Fluid Dynamics*, 20(10): 687–699, 2006.
[10] G. Grötzbach, "Direct Numerical and Large Eddy Simulation of Turbulent Channel Flows", in N.P. Cheremisinoff (Editor), *Encyclopedia of Fluid Mechanics*. West Orange, NJ, 1987.
[11] E. Balaras, C. Benocci, U. Piomelli, "Two-Layer Approximate Boundary Conditions for Large-Eddy Simulations", *AIAA Journal*, 34(6): 1111–1119, June 1996.
[12] W. Cabot, P. Moin, "Approximate Wall Boundary Conditions in the Large-Eddy Simulation of High Reynolds Number Flow", *Flow, Turbulence and Combustion*, 63(1–4): 269–291, January 1999.
[13] M. Wang, P. Moin, "Dynamic Wall Modeling for Large-Eddy Simulation of Complex Turbulent Flows", *Physics of Fluids*, 14(7): 2043–2051, July 2002.
[14] L.J. Souverein, P. Dupont, J.F. Debieve, J.P. Dussauge, B.W. van Oudheusden, F. Scarano, "Effect of Interaction Strength on Unsteadiness in Turbulent Shock-Wave-Induced Separations", *AIAA Journal*, 48(7): 1480–1493, July 2010.
[15] L.J. Souverein, *On The Scaling and Unsteadiness of Shock Induced Separation*, PhD thesis, Delft University of Technology, March 2010.
[16] S. Piponniau, J.P. Dussauge, J.F. Debieve, P. Dupont, "A Simple Model for Low-Frequency Unsteadiness in Shock-Induced Separation", *Journal of Fluid Mechanics*, 629: 87–108, 2009.
[17] S. Kawai, J. Larsson, "Wall-Modeling in Large Eddy Simulation: Length Scales, Grid Resolution, and Accuracy", *Physics of Fluids*, 24(1): 015105, January 2012.
[18] S.K. Lele, "Compact Finite Difference Schemes with Spectral-like Resolution", *Journal of Computational Physics*, 103(1): 16–42, 1992.
[19] S. Obayashi, K. Fujii, S. Gavali, "Navier-Stokes Simulation of Wind-Tunnel Flow Using LU-ADI Factorization Algorithm", NASA-TM-100042, NASA, February 1988.
[20] N. Iizuka, *Study of Mach Number Effect on the Dynamic Stability of a Blunt Re-entry Capsule*, PhD thesis, University of Tokyo, February 2006.
[21] D.P. Rizzetta, M.R. Visbal, G.A. Blaisdell, "A Time-Implicit High-Order Com-

pact Differencing and Filtering Scheme for Large-Eddy Simulation", *International Journal for Numerical Methods in Fluids*, 42(6): 665–693, June 2003.

[22] S. Kawai, S.K. Lele, "Localized Artificial Diffusivity Scheme for Discontinuity Capturing on Curvilinear Meshes", *Journal of Computational Physics*, 227(22): 9498–9526, November 2008.

[23] S. Kawai, S.K. Shankar, S.K. Lele, "Assessment of Localized Artificial Diffusivity Scheme for Large-Eddy Simulation of Compressible Turbulent Flows", *Journal of Computational Physics*, 229(5): 1739–1762, March 2010.

[24] S. Kawai, S.K. Lele, "Large-Eddy Simulation of Jet Mixing in Supersonic Crossflows", *AIAA Journal*, 48(9): 2063–2083, September 2010.

[25] G. Urbin, D. Knight, "Large-Eddy Simulation of a Supersonic Boundary Layer Using an Unstructured Grid", *AIAA Journal*, 39(7): 1288–1295, July 2001.

[26] P. Moin, K. Squires, W. Cabot, S. Lee, "A Dynamic Subgrid-Scale Model for Compressible Turbulence and Scalar Transport", *Physics of Fluids A*, 3(11): 2746–2757, November 1991.

[27] D.K. Lilly, "A Proposed Modification of the Germano Subgrid-Scale Closure Method", *Physics of Fluids A*, 4(3): 633–635, 1992.

[28] S.B. Pope, *Turbulent Flows*, Cambridge University Press, 2000.

[29] S. Kawai, J. Larsson, "A Dynamic Wall Model for Large-Eddy Simulation of High Reynolds Number Compressible Flows", in *CTR Annual Research Briefs 2010*, pages 25–37. Center for Turbulence Research, NASA Ames and Stanford University, 2010, http://www.stanford.edu/group/ctr/ResBriefs/ARB10.html.

[30] D.B. DeGraaff, J.K. Eaton, "Reynolds-Number Scaling of the Flat-Plate Turbulent Boundary Layer", *Journal of Fluid Mechanics*, 422: 319–346, 2000.

[31] S. Pirozzoli, M. Bernardini, "Direct Numerical Simulation Database for Impinging Shock Wave/Turbulent Boundary-Layer Interaction", *AIAA Journal*, 49(6): 1307–1312, June 2010.